Sensors & Actuators: B. Chemical 273 (2018) 185–190

Contents lists available at ScienceDirect

Sensors and Actuators B: Chemical

journal homepage: www.elsevier.com/locate/snb

# A fluorescent biosensor based on molybdenum disulfide nanosheets and protein aptamer for sensitive detection of carcinoembryonic antigen

Lianjing Zhao, Ming Cheng, Guannan Liu, Huiying Lu, Yuan Gao*, Xu Yan, Fangmeng Liu, Peng Sun, Geyu Lu*

*State Key Laboratory on Integrated Optoelectronics, College of Electronic Science and Engineering, Jilin University, 2699 Qianjin Street, Changchun 130012, China*

ARTICLE INFO

*Keywords:*
Molybdenum disulfide ($MoS_2$)
Aptamer
Carcinoembryonic antigen (CEA)
Fluorescent biosensor

ABSTRACT

Simple, rapid, sensitive detection of tumor biomarker carcinoembryonic antigen (CEA) is of great importance for the screening, diagnosis and prognosis evaluation of various gastroenteric tumor. This paper presents a "turn-on" fluorescent biosensor based on molybdenum disulfide ($MoS_2$) nanosheets and fluorophore labeled protein aptamer for rapid and sensitive detection of CEA protein. CEA aptamer probe can be adsorbed on the surface of $MoS_2$ nanosheets in close proximity via van der Waals force, triggering fluorescence resonance energy transfer, and consequently fluorescence signal of aptamer probe was quenched. While in the presence of CEA protein, the fluorescence signal was recovered because aptamer probe could detach from $MoS_2$ nanosheets with binding-induce conformation change. $MoS_2$ nanosheets with high quenching efficiency combined with well discrimination ability between aptamer and aptamer/protein afforded the biosensor easy construction, fast detection and high sensitivity. The sensing platform also exhibited good reproducibility, selectivity and showed high sensitivity for CEA protein in a broad range of 100 pg/mL–100 ng/mL with the detection limit of 34 pg/mL. The aptamer-$MoS_2$ based fluorescent biosensor may be an ideal mode for protein detection in clinical sample, pesticide detection and environmental monitoring.

## 1. Introduction

Cancer is a major worldwide public health problem and the second leading cause of death globally [1]. The cure rate is very low in the middle and late stage, however, it is high at the early stage [2–4]. Therefore, early detection and treatment are significantly important strategy for conquering cancer. Highly sensitive detection of tumor markers may dramatically improve the accuracy rate of cancer early diagnosis. Carcinoembryonic antigen (CEA) is one of the most common tumor biomarkers in clinic, which used for screening, diagnosis and prognosis evaluation of various gastroenteric tumor including colorectal cancer, Esophageal cancer, gastric carcinoma, pancreatic carcinoma [5–8]. So rapid and sensitive detection of CEA is considerably essential for cancer diagnosis and treatment.

At present, the clinical methods of CEA protein detection mainly include enzyme-linked immunosorbent assay (ELISA), radioimmunoassay (RIA) and chemiluminescent immunoassay (CLIA). The electrochemical [9], photochemical [10] and fluorescence analysis method were employed for the development of ultrasensitive CEA immunosensor with excellent sensing properties. However, anti-CEA antibody used in immunoassay has the nature of relatively high cost and easy denaturation. Aptamers as promising alternative of antibody are attractive for the construction of biosensor due to their good stability, ease of synthesis and modification, low cost, fast tissue penetration and low toxicity [11,12]. Therefore, it is highly desirable to develop aptamer-based biosensors for tumor biomarkers detection with easy construction, high sensitivity and stability, as well as low cost. Besides, fluorescent biosensor has drawn much attention and was widely employed to detect protein because of its simplicity, rapid analysis, low-cost and high sensitivity [13–15].

In the past few years, much focus has been paid to graphene oxide (GO) in the construction of fluorescent biosensor due to its high quenching ability and water solubility [16,17]. The sensing platform based on GO has been used to detect many biomolecules [18,19]. Recently, other 2D nanomaterials were continuously discovered and synthesized such as transition metal dichalcogenides (TMDs), transition metal oxides (TMOs), silicate clays, layered double hydroxides (LDHs) [20]. Among them, $MoS_2$ nanosheets share some common features with graphene in structural and physical/chemical properties [21]. $MoS_2$ nanosheets have some special and fascinating properties [22]. First, $MoS_2$ nanosheets have ultrahigh surface-to-volume ratio and can load various and large amounts of biomolecules [23]. Second, $MoS_2$

* Corresponding authors.
*E-mail addresses:* gaoyuan@jlu.edu.cn (Y. Gao), lugy@jlu.Edu.cn (G. Lu).

https://doi.org/10.1016/j.snb.2018.06.004
Received 16 January 2018; Received in revised form 22 May 2018; Accepted 1 June 2018
Available online 02 June 2018
0925-4005/ 

nanosheets exhibit super quenching ability [24]. Third, due to lack of dangling bonds, $MoS_2$ nanosheets show high stability in aqueous solution without the process of surfactants or oxidation treatment [23–28]. All above characteristics make it an ideal candidate as a new nanomaterials in the construction of fluorescent biosensor. In addition, much focus has been also paid on their applications in the biomedical field, including ultrasensitive biosensing, biological imaging, cancer therapy, antibacterial treatment and drug delivery [29–32].

In order to simple, rapid, sensitive and selective detection of CEA, a fluorescence turn-on biosensor based on aptamer-$MoS_2$ nanosheets was established. The sensing platform has a high sensitivity and selectivity for CEA protein, due to the super quenching ability of $MoS_2$ nanosheets and high selective aptamer. The system has merits of fast detection, low cost and easy construction, which make it a promising sensing platform for protein detection in vitro applications.

## 2. Materials and methods

### 2.1. Materials and apparatus

Molybdenum disulfide ($MoS_2$) nanosheets were purchased from Nanjing XF Nano Material Tech Co., Ltd. (Nanjing, China). Carcinoembryonic antigen (CEA) was purchased from Shanghai Linc-Bio Science Co., Ltd (Shanghai, China). Bovine serum albumin (BSA) and immunoglobulins G (IgG) were purchased from Dingguo Biotech Co., Ltd (Beijing, China). Tris-HCl was purchased from Dingguo Biotech Co., Ltd. CEA aptamer probe (CA) and ssDNA were synthesized and purified by Sangon BiotechCo., Ltd (Shanghai, China). The sequence used as follows: CEA aptamer probe (CA) 5′-Texas Red –ATACCAGCT TATTCAATT-3′, random ssDNA 5′-TCATTACATGTTTCCTTACTTC CAG-3′.

The buffer used in this work was 10 mM Tris-HCl (pH 7.4), containing 100 mM NaCl, 5 mM KCl and 5 mM $MgCl_2$. All chemicals were of analytical grade and used without further purification. All solutions were prepared in Milli-Q water (resistance > 18 MΩ cm). All fluorescence measurements were carried out on a RF-5301PC fluorophotometer (Shimadzu, Japan). Time decay photoluminescence measurements were recorded with an Edinburgh FLS920 phosphorimeter (Edinburgh Instruments, U.K.).

### 2.2. Optimization of detection conditions

Firstly, the content of $MoS_2$ nanosheets employed in sensing platform was optimized. The typical procedure was conducted as follow. A certain concentration of $MoS_2$ nanosheets was added to the 5 nM fluorophore-labeled CEA aptamers, followed by the incubation for 10 min at room temperature. The fluorescence spectra were recorded immediately by RF-5301PC fluorophotometer. Meanwhile, 5 nM fluorophore-labeled CA was incubated with 10 ng/mL CEA at 37 °C for 2 h prior to the addition of different concentrations of $MoS_2$ nanosheets. After the incubation for 10 min at room temperature, the fluorescence spectrum was recorded immediately. Each experiment was repeated three times.

In order to determine the quench time of $MoS_2$ nanosheets for CA and CA/CEA, the fluorescence spectra were recorded at different time after the $MoS_2$ nanosheets (200 μg/mL) were added in the 5 nM CA and the mixture of 5 nM CA and 10 ng/mL CEA respectively.

All the experiments were conducted in a buffer solution (10 mM Tris-HCl, containing 100 mM NaCl, 5 mM KCl and 5 mM $MgCl_2$).

### 2.3. Procedures for CEA detection

For CEA detection, 5 nM CA was incubated with different concentrations of CEA at 37 °C for 2 h, and then 200 μg/mL $MoS_2$ nanosheets was added in the same solutions. After the incubation for 10 min at room temperature, the fluorescent intensity changes were recorded on a RF-5301PC fluorophotometer. Fluorescence measurements were performed under the same conditions at the room temperature. The excitation/emission wavelengths were fixed at 595 and 608 nm respectively. To examine the specificity of fluorescent biosensor for CEA protein detection, BSA (10 ng/mL and 40 ng/mL), IgG (10 ng/mL and 40 ng/mL), ssDNA (10 nM) were added into the system instead of CEA respectively followed by the same CEA detection procedure.

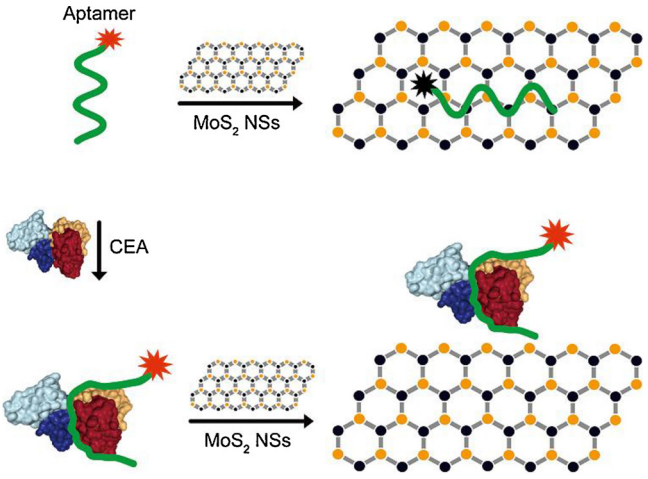


**Fig. 1.** Schematic illustration of fluorescent biosensor based on $MoS_2$ nanosheets for CEA protein detection.

## 3. Results and discussion

### 3.1. Mechanism of fluorophore-labeled aptamer/$MoS_2$ based FRET biosensor

The mechanism of fluorescent bio-sensing system biosensor for CEA detection in this work is illustrated in Fig. 1. Fluorophore (Texas Red) was used as fluorescence resonance energy transfer (FERT) donor, which can emit intense blue light at 608 nm under light excitation of 595 nm. $MoS_2$ nanosheets were served as FERT acceptors owing to high fluorescence quenching ability. Fluorophore-labeled aptamer can adsorb on the surface of $MoS_2$ nanosheets in close proximity via van der Waals force between nucleobases and the basal pane of $MoS_2$ nanosheets [24,25,33], furthermore, FRET between fluorophore and $MoS_2$ nanosheets was triggered, resulting in the subsequent fluorescence quenching of the fluorophore. In contrast, when CEA existed in the reaction system, they would bind with CA, resulting in the change of conformation of CA/CEA complex. Therefore, the interaction between CA/CEA complex and $MoS_2$ nanosheets became so weak that CA detached from the surface of $MoS_2$ nanosheets, leading to the restoration of fluorescence signal. Consequently, the target CEA protein can be detected by monitoring the variation of fluorescence signal.

### 3.2. Construction of biosensor based on $MoS_2$ nanosheets and protein aptamer

To investigate the feasibility of fluorophore-labeled aptamer/$MoS_2$ based FRET biosensor, the fluorescence spectra of CA and CA/ CEA in the absence or presence of $MoS_2$ nanosheets were recorded respectively. As shown in Fig. 2, CA and CA/CEA exhibit the similar fluorescence in the absence of $MoS_2$ nanosheets, which demonstrates that the interaction between CA and CEA hardly had an effect on the fluorescence intensity of CA. Moreover, the fluorescence intensity of CA could be quenched 99.1% by optimal concentration of $MoS_2$ nanosheets (200 μg/mL) (green curve) and restored dramatically by addition of target CEA protein (blue curve). These results indicate that $MoS_2$ nanosheets not only possess high fluorescence quenching ability to CA but also have

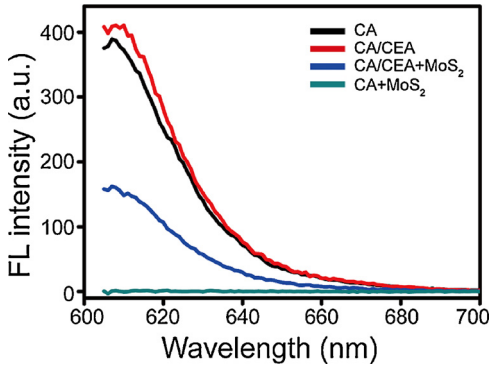


**Fig. 2.** Fluorescence spectra of CA under different conditions: CA (black curve), CA/CEA (red curve); CA/CEA + $MoS_2$ nanosheets (blue curve); CA + $MoS_2$ nanosheets (green curve). The concentrations of CA and CEA are 5 nM and 10 ng/mL respectively. The excitation and emission wavelengths are 595 and 608 nm respectively. (For interpretation of the references to colour in this figure legend, the reader is referred to the web version of this article.)

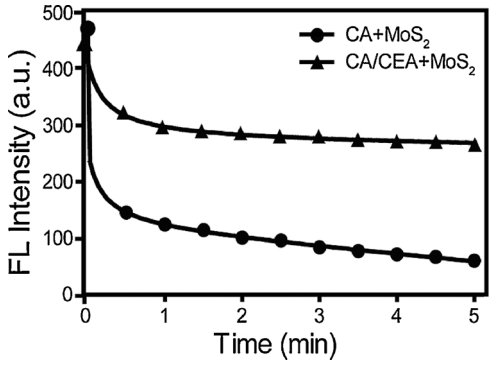


**Fig. 3.** The fluorescence quenching curves for CA and CA/CEA in the presence of $MoS_2$nanosheets. The concentrations of CA and CEA are 5 nM and 10 ng/mL respectively. The excitation and emission wavelengths are 595 and 608 nm respectively.

well discrimination ability between CA and CA/CEA, which guarantee a lower fluorescence background signal and sensitive response for target CEA protein. In addition, these results reveal that the affinity between CA and $MoS_2$ nanosheet is apparently lower than that between CA and target protein CEA. As shown in Fig. 3, the fluorescence quenching of both CA and CA/CEA by $MoS_2$ nanosheets is very fast. Most of fluorescence is rapidly quenched within about 1 min, Furthermore, reached equilibrium within about 5 min. This also verifies the excellent quenching ability of $MoS_2$ nanosheets and different affinities of $MoS_2$ nanosheets for CA and CA/CEA.

To establish the sensitive biosensor, effectively quenching the fluorescence of CA by $MoS_2$ nanosheets and restoring the fluorescence of CA by adding the target protein, we optimized the ratio of the $MoS_2$ nanosheets to the CA. Firstly, the quenching ability of $MoS_2$ nanosheets for CA was determined. 5 nM CA was mixed with different concentrations of $MoS_2$ nanosheets ranging from 0 μg/mL to 400 μg/mL. The fluorescence signal changes were recorded by fluorophotometer. As shown in Fig. 4, the fluorescence intensity of CA gradually decreases with increase in concentrations of $MoS_2$ nanosheets and almost reaches the baseline level with 99.1% quenching efficiency when the concentration of $MoS_2$ nanosheets is 200 μg/mL. The fluorescence quenching efficiency is calculated by the equation of $QE = (F_0 - F_q)/F_0$, where $F_0$ stands for the initial fluorescence intensity of fluorescence labeled aptamer, and $F_q$ stands for the fluorescence intensity of fluorescence labeled aptamer which has been quenched by $MoS_2$ nanosheets. Afterwards, the fluorescence signal changes very little when the concentration of $MoS_2$ nanosheets continued to increase. Furthermore, the

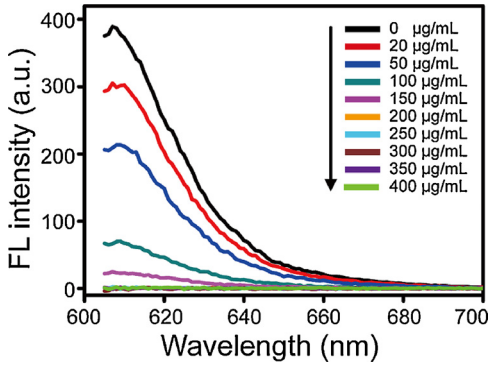


**Fig. 4.** The fluorescence spectra of CA in presence of different concentrations of $MoS_2$ nanosheets. Excitation wavelength: 595 nm, CA: 5 nM, $MoS_2$ nanosheets concentration range: 0–400 μg/mL.

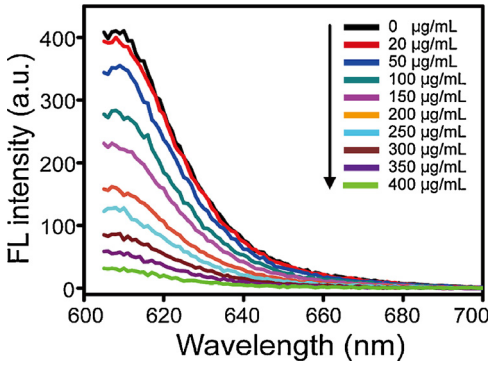


**Fig. 5.** The fluorescence spectra of CA/CEA in presence of different concentrations of $MoS_2$ nanosheets. Excitation wavelength: 595 nm, CA: 5 nM, CEA: 10 ng/mL, $MoS_2$ nanosheets concentration range: 0–400 μg/mL.

fluorescence signal in the presence of target protein was also monitored after different concentrations of $MoS_2$ nanosheets were added respectively, which results are shown in Fig. 5. 5 nM CA was incubated with 10 ng/mL CEA protein at 37 °C for 2 h, followed by incubation with the same concentrations of $MoS_2$ nanosheets ranging from 0 μg/mL to 400 μg/mL. The fluorescence signal was measured by the same condition. The fluorescence intensity gradually decreases with increase in concentrations of $MoS_2$ nanosheets. However, the fluorescence intensity all recoveries to varying extent by comparing with that of absence of target protein under the same concentration of $MoS_2$ nanosheets. What's more, we analyzed the effect of $MoS_2$ concentration on the fluorescence recovery extent, discussing the difference of fluorescence intensity at 608 nm between CA/CEA and CA after addition of different concentrations of $MoS_2$ nanosheets. Fig. 6 shows the extent of fluorescence recovery first increases and then decreases along with the increase in the concentration of $MoS_2$ nanosheets (red column). In addition, the fluorescence signal recovered at maximum level when $MoS_2$ nanosheets concentration was 100, 150 and 200 μg/mL respectively. By comparison, the fluorescence background signal, the fluorescence at the absence of target protein, was the lowest of the three at the $MoS_2$ nanosheets concentration of 200 μg/mL (black column). Therefore, the $MoS_2$ nanosheets concentration of 200 μg/mL was chosen for the following CEA detection experiments, which simultaneously ensured the low fluorescence background signal (99.1% quenching efficiency) and high degree of fluorescence recovery.

### 3.3. Detection of CEA

The established biosensor based on $MoS_2$ nanosheets and protein aptamer was utilized to detect CEA protein with the optimized $MoS_2$ nanosheets concentration of 200 μg/mL. Different concentrations of

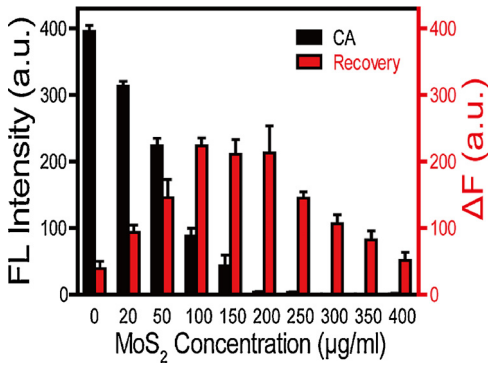


**Fig. 6.** The fluorescence intensity at 608 nm of CA in presence of different concentrations of $MoS_2$ nanosheets (black column) and the fluorescence recovery intensity at 608 nm after addition of target protein CEA in presence of different concentrations of $MoS_2$ nanosheets (red column). (For interpretation of the references to colour in this figure legend, the reader is referred to the web version of this article.)

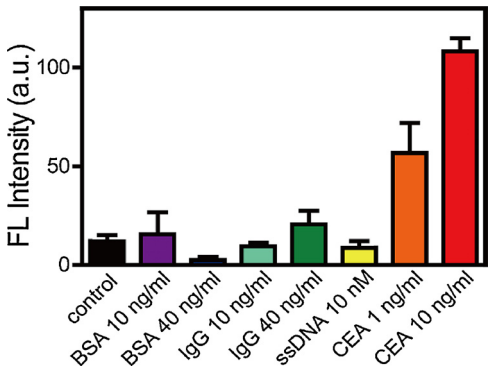


**Fig. 8.** Selectivity of $MoS_2$-aptamer probe based biosensor with BSA, IgG and ssDNA as control groups. All error bars were estimated from three replicate measurements.

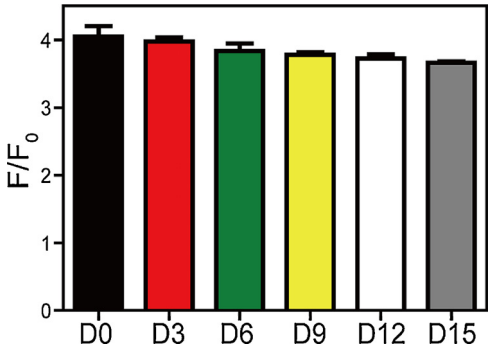


**Fig. 9.** The stability of $MoS_2$-aptamer probe based biosensor.

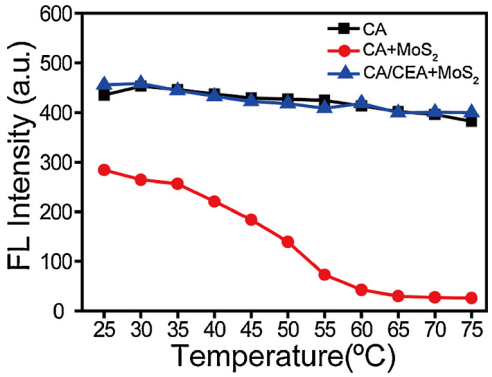


**Fig. 10.** The influence of temperature on the sensing performance.

CEA protein were incubated with 5 nM CA prior to the addition of $MoS_2$ nanosheets (200 μg/mL) respectively. As shown in Fig. 7(a), the fluorescence signal is gradually increasing with the increasing concentrations of target CEA protein and the maximum fluorescence intensity is observed when the concentration of target CEA is greater than or equal to 80 u g/mL. The fluorescence signal changes very little when the concentration of CEA protein continued to increase (Fig. 7(a) and (b)). The fluorescence signal recovery is owing to the strong affinity of target protein for aptamer, leading to desorption of aptamer from $MoS_2$ nanosheets surface. The FRET between fluorphore labeled aptamer and $MoS_2$ nanosheets is hampered as the distance between the two components increased. Fig. 7(b) shows the fluorescence intensity ratio $F/F_0$ increased with the increasing CEA concentration. F and $F_0$ stand for the fluorescence intensity of aptamers/$MoS_2$ nanosheets at 608 nm in the presence and absence of CEA protein respectively. As shown in the inset of Fig. 7(b), a good linear correlation was achieved between the $F/F_0$ and logarithmic concentrations of CEA protein in a wide range of 0.1–100 ng/mL. The linear regression equation could be fitted to $F/F_0 = 6.8408 + 6.78455 \log [CEA]$ ($R^2 = 0.9828$, n = 10). The limit of detection (LOD) is 34 pg/mL (S/N = 3). Compared with analytical performance of other homogeneous CEA biosensor, the proposed biosensor exhibited a similar or better analytical performance [12,34]. The LOD and the linear range is better than that of fluorescent biosensor based on quantum dots and gold nanoparticles for CEA detection with LOD of 300 pg/mL and detection range of 1–100 ng/mL [34]. The analytical performance is similar to that of fluorescent biosensor for indirectly detecting CEA (linear range of 0.05–20 ng/mL with a limit of detection of 6.7 pg/mL [12]. Moreover, the LOD of the proposed biosensor is far lower than the threshold value in normal human serum (3 ng/mL) [35]. The high sensitivity suggests the potential application

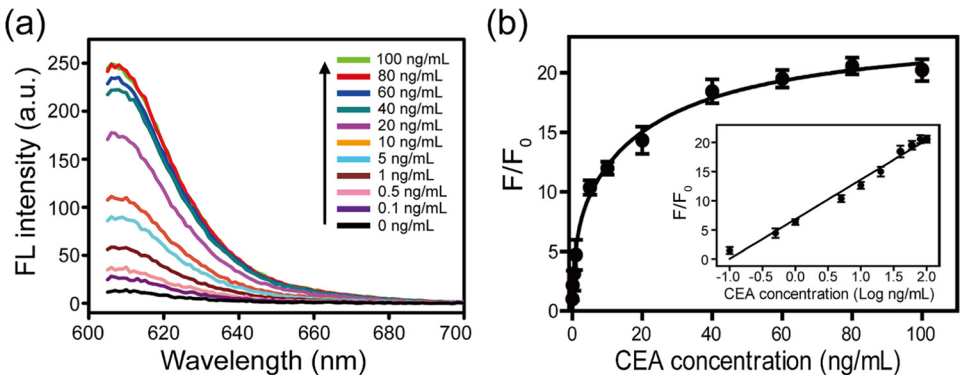


**Fig. 7.** (a) Fluorescence spectra of $MoS_2$-aptamer probe based biosensor in the presence of different concentrations of CEA. (b) The sensitivity analysis of $MoS_2$-aptamer probe based biosensor between different concentrations of CEA and fluorescence intensity ratio $F/F_0$. Inset shows calibration curve between $F/F_0$ and logarithmic concentrations of CEA. F and $F_0$ stand for the fluorescence intensity of aptamer/$MoS_2$ nanosheets at 608 nm in the presence and absence of CEA protein respectively. All error bars were estimated from three replicate measurements.

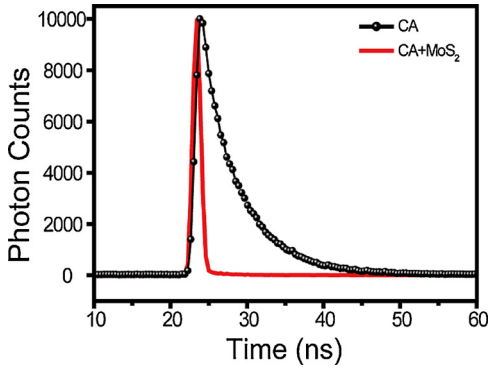


**Fig. 11.** The fluorescence decay curve of the CA and CA/$MoS_2$ nanosheets.

of our aptamer functional fluorescence biosensor based on $MoS_2$ nanosheets for CEA protein detection.

### 3.4. Selectivity and stability of $MoS_2$-aptamer probe based biosensor

To evaluate the specificity of the sensing platform, the responses of the biosensor to interferences, different concentrations of BSA, IgG and random single strand DNA, were measured under the same experiment conditions as CEA detection. Fig. 8 shows that the fluorescence intensity of control groups is more close to blank and significantly lower than that of 1 ng/mL CEA, especially that of 10 ng/mL CEA. These results suggest that the biosensor platform has excellent selectivity for CEA protein, which is attributed to the high selectivity of the aptamer.

The stability of the biosensor is another important element for the application. The stability of CA/$MoS_2$ nanosheets was studied during a 15-day period, which was evaluated by assaying the same CEA concentration (5 ng/mL) intermittently (every 3 days). Fig.9 shows that little change in the fluorescence intensity was found after storage for 15 days, but only 9.5% decrease in the initial signal was noticed after 15 days. The reason may be the fact that the quenching efficiency of $MoS_2$ nanosheets for CA was slightly decreased during the storage.

### 3.5. The influence of temperature on the sensing performance

The effect of temperature on the sensing performance was investigated by measuring the fluorescence intensity of CA, CA/$MoS_2$ nanosheets and CA/CEA/$MoS_2$ system respectively at different temperature. The temperature was regularly changed from 25 °C to 75 °C with interval of 5 °C. Fig.10 shows fluorescence intensity of both CA and CA/CEA/$MoS_2$ have no obvious decrease, while fluorescence intensity of CA/$MoS_2$ system decreases sharply with the increasing temperature and is almost quenched completely over 65 °C. Results indicate that the increase of reaction temperature results in an increase of the quenching efficiency of $MoS_2$ nanosheets to the labeled Texas Red, in the range from 25 °C to 65 °C, which is the observation of dynamic quenching process. Although the interaction between DNA aptamer and $MoS_2$ nanosheets was attributed to van der Waals force, which reported in relative literature [24,25,33], the labeled Texas Red fluorescence featured a dynamic quenching process with the interaction of $MoS_2$ nanosheets. Since dynamic quenching is related to diffusion, higher temperature accelerated the thermal motion of nanomaterials and augmented effective collision between nanosheets and Texas Red, leading to increased quenching efficiency. The dynamic quenching mechanism is also confirmed by measurement of the fluorescence lifetime. The fluorescence lifetime of aptamer in the absence and presence of $MoS_2$ nanosheets was measured by an Edinburgh FLS920 phosphorimeter. As shown in Fig. 11, the decay curve of CA and CA/$MoS_2$ nanosheets can be fitted by single exponential and double exponential behavior respectively. The lifetime of CA in the presence of $MoS_2$ nanosheets ($0.324*10^{-9}$) was obviously shorter than that of free CA ($4.976*10^{-9}$). This result further indicated the fluorescence quenching process belongs to the dynamic quenching mechanism.

## 4. Conclusion

The sensitive and specific biosensor based on $MoS_2$ nanosheets and aptamer probes for CEA detection was established. $MoS_2$ nanosheets with high fluorescence quenching ability and well discrimination toward the CA and CA/CEA afford the biosensor easy construction, fast detection and high sensitivity. CA can easily be adsorbed on the surface of $MoS_2$ nanosheets and fast quenched by $MoS_2$ nanosheets consequently. The fluorescence restoration of the sensing system was observed in the presence of target CEA protein. The fluorescence quenching mechanism belongs to the dynamic quenching in this investigation. After optimizing, the sensing platform was successfully utilized to detect target CEA protein, which exhibited the linear response range within 0.1–100 ng/mL and the detection limit of 34 pg/mL. Moreover, the sensing system had a better specificity for CEA than interference proteins and random single strand DNA. These results demonstrate $MoS_2$/CA based biosensor has the potential to be a stable and cheap sensing platform for CEA detection. The methodology in this work can be easily adapted to detect other proteins.

## Acknowledgments

This work was supported by grants from the National Nature Science Foundation of China (61304242, 61520106003), National High-Tech Research and Development Program of China (863 Program, No. 2014AA06A505).

## References

[1] M. Noor, V. Narwal, Machine Learning Approaches in Cancer Detection and Diagnosis: Mini Review, (2017).
[2] P.A. Crosbie, R. Shah, Y. Summers, C. Dive, F. Blackhall, Prognostic and predictive biomarkers in early stage NSCLC: CTCs and serum/plasma markers, Transl. Lung Cancer Res. 2 (2013) 382–397.
[3] D.R. Aberle, A.M. Adams, C.D. Berg, W.C. Black, J.D. Clapp, R.M. Fagerstrom, et al., Reduced lung-cancer mortality with low-dose computed tomographic screening, N. Engl. J. Med. 365 (2011) 395.
[4] Y.W. Xu, Y.H. Peng, B. Chen, Z.Y. Wu, J.Y. Wu, J.H. Shen, et al., Autoantibodies as potential biomarkers for the early detection of esophageal squamous cell carcinoma, Am. J. Gastroenterol. 109 (2014) 36–45.
[5] N. Beauchemin, A. Arabzadeh, Carcinoembryonic antigen-related cell adhesion molecules (CEACAMs) in cancer progression and metastasis, Cancer Metastasis Rev. 32 (2013) 643–671.
[6] Y. Xiao, J. Zhang, X. He, J. Ji, G. Wang, Diagnostic values of carcinoembryonic antigen in predicting peritoneal recurrence after curative resection of gastric cancer: a meta-analysis, Ir. J. Med. Sci. 183 (2014) 557–564.
[7] M. Lukaszewicz-Zajac, B. Mroczko, M. Kozlowski, J. Niklinski, J. Laudanski, M. Szmitkowski, Higher importance of interleukin 6 than classic tumor markers (carcinoembryonic antigen and squamous cell cancer antigen) in the diagnosis of esophageal cancer patients, Dis. Esophagus 25 (2012) 242–249.
[8] C. Liu, H. Ma, L. Qu, J. Wu, L. Meng, C. Shou, Elevated serum synuclein-gamma in patients with gastrointestinal and esophageal carcinomas, Hepatogastroenterology 59 (2012) 2222–2227.
[9] Y. Wang, G. Zhao, Y. Zhang, X. Pang, W. Cao, B. Du, et al., Sandwich-type electrochemical immunosensor for CEA detection based on Ag/MoS 2 @Fe 3 O 4 and an analogous ELISA method with total internal reflection microscopy, Sens. Actuators B: Chem. 266 (2018) 561–569.
[10] Q. Han, R. Wang, B. Xing, T. Zhang, M.S. Khan, D. Wu, et al., Label-free photoelectrochemical immunoassay for CEA detection based on CdS sensitized WO3@BiOI heterostructure nanocomposite, Biosens. Bioelectron. 99 (2018) 493–499.
[11] J. Shi, J. Lyu, F. Tian, M. Yang, A fluorescence turn-on biosensor based on graphene quantum dots (GQDs) and molybdenum disulfide (MoS2) nanosheets for epithelial cell adhesion molecule (EpCAM) detection, Biosens. Bioelectron. 93 (2017) 182–188.
[12] Z. Qiu, J. Shu, D. Tang, Bioresponsive release system for visual fluorescence detection of carcinoembryonic antigen from mesoporous silica nanocontainers mediated optical color on quantum dot-enzyme-impregnated paper, Anal. Chem. 89 (2017) 5152–5160.
[13] Y. He, Y. Lin, H. Tang, D. Pang, A graphene oxide-based fluorescent aptasensor for the turn-on detection of epithelial tumor marker mucin 1, Nanoscale 4 (2012) 2054–2059.
[14] S. Zhu, Z. Liu, L. Hu, Y. Yuan, G. Xu, Turn-on fluorescence sensor based on single-walled-carbon-nanohorn-peptide complex for the detection of thrombin, Chemistry

18 (2012) 16556–16561.
[15] S. Zhu, S. Han, L. Zhang, S. Parveen, G. Xu, A novel fluorescent aptasensor based on single-walled carbon nanohorns, Nanoscale 3 (2011) 4589–4592.
[16] Y. Wen, C. Peng, D. Li, L. Zhuo, S. He, L. Wang, et al., Metal ion-modulated graphene-DNAzyme interactions: design of a nanoprobe for fluorescent detection of lead(ii) ions with high sensitivity, selectivity and tunable dynamic range, Chem. Commun. 47 (2011) 6278.
[17] M. Liu, H. Zhao, S. Chen, H. Yu, Y. Zhang, X. Quan, A "turn-on" fluorescent copper biosensor based on DNA cleavage-dependent graphene-quenched DNAzyme, Biosens. Bioelectron. 26 (2011) 4111–4116.
[18] C.H. Lu, H.H. Yang, C.L. Zhu, X. Chen, G.N. Chen, A graphene platform for sensing biomolecules, Angew. Chem. Int. Ed. Engl. 48 (2009) 4785–4787.
[19] H. Chang, L. Tang, Y. Wang, J. Jiang, J. Li, Graphene fluorescence resonance energy transfer aptasensor for the thrombin detection, Anal. Chem. 82 (2010) 2341.
[20] D. Chimene, D.L. Alge, A.K. Gaharwar, Two-dimensional nanomaterials for biomedical applications: emerging trends and future prospects, Adv. Mater. 27 (2015) 7261–7284.
[21] M. Chhowalla, H.S. Shin, G. Eda, L.J. Li, K.P. Loh, H. Zhang, The chemistry of two-dimensional layered transition metal dichalcogenide nanosheets, Nat. Chem. 5 (2013) 263–275.
[22] X. Li, J. Shan, W. Zhang, S. Su, L. Yuwen, L. Wang, Recent advances in synthesis and biomedical applications of two-dimensional transition metal dichalcogenide nanosheets, Small 13 (2017).
[23] K. Kalantar-zadeh, J.Z. Ou, T. Daeneke, M.S. Strano, M. Pumera, S.L. Gras, Two-dimensional transition metal dichalcogenides in biosystems, Adv. Funct. Mater. 25 (2015) 5086–5099.
[24] C. Zhu, Z. Zeng, H. Li, F. Li, C. Fan, H. Zhang, Single-layer MoS2-based nanoprobes for homogeneous detection of biomolecules, J. Am. Chem. Soc. 135 (2013) 5998–6001.
[25] Y. Zhang, B. Zheng, C. Zhu, X. Zhang, C. Tan, H. Li, et al., Single-layer transition metal dichalcogenide nanosheet-based nanosensors for rapid, sensitive, and multiplexed detection of DNA, Adv. Mater. 27 (2015) 935–939.
[26] J.T. Robinson, S.M. Tabakman, Y. Liang, H. Wang, H.S. Casalongue, D. Vinh, et al., Ultrasmall reduced graphene oxide with high near-infrared absorbance for photothermal therapy, J. Am. Chem. Soc. 133 (2011) 6825–6831.
[27] K. Yang, J. Wan, S. Zhang, B. Tian, Y. Zhang, Z. Liu, The influence of surface chemistry and size of nanoscale graphene oxide on photothermal therapy of cancer using ultra-low laser power, Biomaterials 33 (2012) 2206–2214.
[28] H. Fang, C. Battaglia, C. Carraro, S. Nemsak, B. Ozdol, J.S. Kang, et al., Strong interlayer coupling in van der Waals heterostructures built from single-layer chalcogenides, Proc. Natl. Acad. Sci. U. S. A. 111 (2014) 6198.
[29] T. Liu, C. Wang, X. Gu, H. Gong, L. Cheng, X. Shi, et al., Drug delivery with PEGylated MoS2 nano-sheets for combined photothermal and chemotherapy of cancer, Adv. Mater. 26 (2014) 3433–3440.
[30] M. Pumera, A.H. Loo, Layered transition-metal dichalcogenides (MoS2 and WS2) for sensing and biosensing, TrAC, Trends Anal. Chem. 61 (2014) 49–53.
[31] K. Kalantar-zadeh, J.Z. Ou, Biosensors based on two-dimensional MoS2, ACS Sens. 1 (2016) 5–16.
[32] L. Cheng, C. Yuan, S. Shen, X. Yi, H. Gong, K. Yang, et al., Bottom-Up synthesis of metal-ion-doped WS2 nanoflakes for cancer theranostics, ACS Nano 9 (2015) 11090.
[33] B.L. Li, H.L. Zou, L. Lu, Y. Yang, J.L. Lei, H.Q. Luo, et al., Size-dependent optical absorption of layered MoS2and DNA oligonucleotides induced dispersion behavior for label-free detection of single-nucleotide polymorphism, Adv. Funct. Mater. 25 (2015) 3541–3550.
[34] J. Qian, C. Wang, X. Pan, S. Liu, A high-throughput homogeneous immunoassay based on Forster resonance energy transfer between quantum dots and gold nanoparticles, Anal. Chim. Acta 763 (2013) 43–49.
[35] X. Chen, X. Jia, J. Han, J. Ma, Z. Ma, Electrochemical immunosensor for simultaneous detection of multiplex cancer biomarkers based on graphene nanocomposites, Biosens. Bioelectron. 50 (2013) 356–361.

**Lianjing Zhao** received her M.S. degree in 2013 from Jilin University, China. She is currently studying for her Ph.D. degree in College of Electronic Science and Engineering, Jilin University. Her research interests mainly focus on the development of the functional nanomaterials and their applications in chem/bio sensor.

**Ming Cheng** received his BE degree from Jilin University of China in 2017. He is currently working toward the MS degree in the Electronics Science and Engineering department, Jilin University. His current researches focus on the preparation and application of graphene and semiconductor oxide, especially in gas sensor.

**Guannan Liu** received his BE degree from Jilin University of China in 2015. He is currently working toward the MS degree in the Electronics Science and Engineering department, Jilin University. His current research is focus on the synthesis of carbon dots and their applications.

**Huiying Lu** received his MS degree from College of Chemistry, Jilin University, China in 2012 and received his PhD degree from College of Chemistry, Jilin University, China in 2015. He is currently studying for his post-doctoral degree in College of Electronic Science and Engineering, Jilin University, China.

**Yuan Gao** received her PhD degree from Department of Analytical Chemistry at Jilin University in 2012. Now she is an associate professor in Jilin University, China. Her current research is focus on the preparation and application of graphene and semiconductor oxide, especial in gas sensor and biosensor.

**Xu Yan** received his M.S degree in 2013 from Nanjing Agricultural University. He joined the group of Prof. Xingguang Su at Jilin University and received his Ph.D. degree in June 2017. Since then, he did postdoctoral work with Prof. Geyu Lu and Prof. Junqiu Liu. Currently, his research interests mainly focus on the development of the functional nanomaterials for chem/bio sensors.

**Fangmeng Liu** received his B.S. degree in 2009 from College of Chemistry, Liaocheng University and M.S. degree in 2012 from Northeast Forestry University in China. Currently he is studying for his Ph.D. degree in College of Electronic Science and Engineering, Jilin University, China.

**Peng Sun** received his PhD degree from College of Electronic Science and Engineering, Jilin University, China in 2014. He was appointed the lecturer in Jilin University in the same year. Now, he is engaged in the synthesis and characterization of the semiconducting functional materials and gas sensors.

**Geyu Lu** received the B.Sci. degree in electronic sciences in 1985 and the M.S. degree in 1988 from Jilin University in China and the Dr. Eng. degree in 1998 from Kyushu University in Japan. Now he is a professor of Jilin University, China. His current research interests include the development of chemical sensors and the application of the function materials.